Regulation of retromer recruitment to endosomes by sequential action of Rab5 and Rab7

Raul Rojas,[1] Thijs van Vlijmen,[3] Gonzalo A. Mardones,[1] Yogikala Prabhu,[1] Adriana L. Rojas,[2] Shabaz Mohammed,[4] Albert J.R. Heck,[4] Graça Raposo,[5] Peter van der Sluijs,[3] and Juan S. Bonifacino[1]

[1]Cell Biology and Metabolism Program, Eunice Kennedy Shriver National Institute of Child Health and Human Development and [2]Laboratory of Molecular Biology, National Institute of Diabetes and Digestive and Kidney Diseases, National Institutes of Health, Bethesda, MD 20892
[3]Department of Cell Biology, University Medical Center Utrecht, 3584 CX Utrecht, Netherlands
[4]Department of Biomolecular Mass Spectrometry, Utrecht University, 3584 CA Utrecht, Netherlands
[5]Institut Curie, Centre National de la Recherche Scientifique, Unité Mixte de Recherche 144, Paris 75248, France

The retromer complex mediates retrograde transport of transmembrane cargo from endosomes to the trans-Golgi network (TGN). Mammalian retromer is composed of a sorting nexin (SNX) dimer that binds to phosphatidylinositol 3-phosphate–enriched endosomal membranes and a vacuolar protein sorting (Vps) 26/29/35 trimer that participates in cargo recognition. The mammalian SNX dimer is necessary but not sufficient for recruitment of the Vps26/29/35 trimer to membranes. In this study, we demonstrate that the guanosine triphosphatase Rab7 contributes to this recruitment. The Vps26/29/35 trimer specifically binds to Rab7–guanosine triphosphate (GTP) and localizes to Rab7-containing endosomal domains. Interference with Rab7 function causes dissociation of the Vps26/29/35 trimer but not the SNX dimer from membranes. This blocks retrieval of mannose 6-phosphate receptors to the TGN and impairs cathepsin D sorting. Rab5-GTP does not bind to the Vps26/29/35 trimer, but perturbation of Rab5 function causes dissociation of both the SNX and Vps26/29/35 components from membranes through inhibition of a pathway involving phosphatidylinositol 3-kinase. These findings demonstrate that Rab5 and Rab7 act in concert to regulate retromer recruitment to endosomes.

Introduction

The retromer is a phylogenetically conserved multisubunit complex that mediates retrograde transport of transmembrane cargo from endosomes to the TGN (Seaman, 2005; Bonifacino and Rojas, 2006; Bonifacino and Hurley, 2008). The best-characterized cargo for the mammalian retromer is the cation-independent mannose 6-phosphate receptor (MPR [CI-MPR]), one of two intracellular sorting receptors that participates in the delivery of acid hydrolases to lysosomes (Kornfeld, 1992). The CI-MPR binds newly synthesized acid hydrolases at the TGN and carries them within clathrin-coated vesicles to endosomes, where the hydrolases are released for eventual transport to lysosomes. The retromer functions to retrieve the unoccupied receptors to the

TGN, where they engage in further cycles of acid hydrolase sorting. Depletion of retromer subunits by RNAi prevents this retrieval, leading to rerouting of the receptors to lysosomes and consequent leakage of newly synthesized acid hydrolases into the extracellular medium (Arighi et al., 2004; Carlton et al., 2004; Seaman, 2004; Rojas et al., 2007).

The mammalian retromer comprises two biogenetically distinct subcomplexes of tightly assembled subunits: a dimer composed of a still undefined combination of sorting nexin 1 (SNX1), SNX2, SNX5, and SNX6 (herein referred to as the SNX subcomplex) and a heterotrimer composed of vacuolar protein sorting 26 (Vps26), Vps29, and Vps35 (the Vps subcomplex; Haft et al., 2000; Collins et al., 2005; Hierro et al., 2007; Rojas et al., 2007). Recent studies have begun to shed light into the structure and function of the different retromer subunits. SNX1, SNX2, SNX5, and SNX6 are members of the SNX family of

R. Rojas and T. van Vlijmen contributed equally to this paper.

Correspondence to P. van der Sluijs: p.vandersluijs@umcutrecht.nl; or J.S. Bonifacino: juan@helix.nih.gov

Abbreviations used in this paper: AP, adapter protein; CI-MPR, cation-independent MPR; GMP-PNP, guanylyl-5′-imidodiphosphate; MPR, mannose 6-phosphate receptor; PI3K, phosphatidylinositol 3-kinase; PI3P, phosphatidylinositol 3-phosphate; SNX, sorting nexin; TfR, transferrin receptor; Vps, vacuolar protein sorting.

The online version of this article contains supplemental material.

THE JOURNAL OF CELL BIOLOGY

proteins (Carlton and Cullen, 2005; Cullen, 2008), which are characterized by the presence of a phox homology domain that binds phosphatidylinositol 3-phosphate (PI3P) and other phosphoinositides (Burda et al., 2002; Cozier et al., 2002; Zhong et al., 2002; Carlton et al., 2005a) and a Bin–Amphiphysin–Rvs domain that mediates dimerization and binding to highly curved membranes (Carlton et al., 2004; Carlton and Cullen, 2005). These properties endow the SNX subcomplex with the ability to bind endosomal membranes independently of the Vps subcomplex (Rojas et al., 2007).

The Vps subcomplex has recently been shown to consist of a 210-Å-long filament comprising one copy each of Vps26, Vps29, and Vps35 (Hierro et al., 2007). At one end of this filament lies Vps26, a protein with structural similarity to the arrestin family of sorting adapters (Shi et al., 2006). The other end comprises Vps29 and the C-terminal half of Vps35 (Hierro et al., 2007). Vps29 has a metallophosphoesterase fold (Collins et al., 2005; Wang et al., 2005) but little or no enzymatic activity (Collins et al., 2005; Hierro et al., 2007; but see Damen et al., 2006) caused by occlusion of the putative active site by the Vps35 C-terminal half and replacement of the key catalytic His residue by a Phe residue in the putative active site (Hierro et al., 2007). This latter domain consists of a horseshoe-shaped α-helical solenoid reminiscent of the trunk domain of adaptins (Hierro et al., 2007). Both ends of the filament are connected by the N-terminal half of Vps35 (Hierro et al., 2007). Molecular electron microscopy of this domain has shown that it consists of an extended α-helical solenoid (Hierro et al., 2007). Several lines of evidence indicate that the Vps subcomplex functions to recognize sorting signals within the cytosolic tails of retrograde cargo such as the MPRs (Nothwehr et al., 1999, 2000; Arighi et al., 2004; Seaman, 2007). The Vps35 subunit, in particular, has been proposed to interact with retrograde sorting signals (Nothwehr et al., 2000; Arighi et al., 2004), although definitive structural evidence for such interactions is still lacking.

The Vps subcomplex does not seem capable of directly interacting with membrane lipids (Collins et al., 2005; Shi et al., 2006). Instead, it requires the SNX subcomplex for recruitment to membranes (Rojas et al., 2007). Indeed, depletion of SNX subcomplex subunits by RNAi results in dissociation of the Vps subcomplex from membranes (Rojas et al., 2007). Interactions between the two subcomplexes have been proposed to occur between the relatively unstructured N-terminal extensions of SNX1 and SNX2 (Gullapalli et al., 2004) and several sites on Vps29 and Vps35 (Haft et al., 2000; Collins et al., 2005). However, in mammalian cells, the SNX and Vps subcomplexes exist as separate entities in cytosolic and detergent extracts of cells (Rojas et al., 2007) and do not seem capable of binding to each other in vitro (Collins et al., 2005; Rojas et al., 2007). In fact, the only evidence for binding of these subcomplexes comes from weak interactions detected in the yeast two-hybrid system (Haft et al., 2000; Rojas et al., 2007) and from coprecipitation of overexpressed proteins (Gullapalli et al., 2004). This indicates that other as yet unidentified factors might contribute to the recruitment of the Vps subcomplex to membranes.

In this study, we report that the small GTPase Rab7 is a regulator of Vps subcomplex recruitment to membranes.

We discovered this role in the course of affinity purification experiments aimed at identifying proteins that interact with endosomal Rabs. Immunoblot analyses revealed the presence of the retromer Vps subcomplex among the proteins eluted from a column of GST-Rab7 loaded with the nonhydrolyzable GTP analogue guanylyl-5′-imidodiphosphate (GMP-PNP). This interaction was guanine nucleotide dependent and specific to Rab7 among other endosomal Rabs. Furthermore, GST pull-down experiments with purified recombinant proteins showed that the interaction between Rab7 and the Vps subcomplex is direct. We went on to demonstrate that the Vps subcomplex localizes to endosomal domains that contain Rab7 and that depletion or dominant-negative interference of Rab7 causes dissociation of the Vps subcomplex from membranes, inhibition of CI-MPR retrograde transport, and missorting of the acid hydrolase cathepsin D. In addition, we found that Rab5 indirectly contributes to the recruitment of retromer to membranes, most likely through activation of a pathway involving the Rab5 effector phosphatidylinositol 3-kinase (PI3K) and the SNX subcomplex. Thus, both Rab5 and Rab7 act in a sequential manner to enable retromer recruitment to endosomes and its function in retrograde traffic.
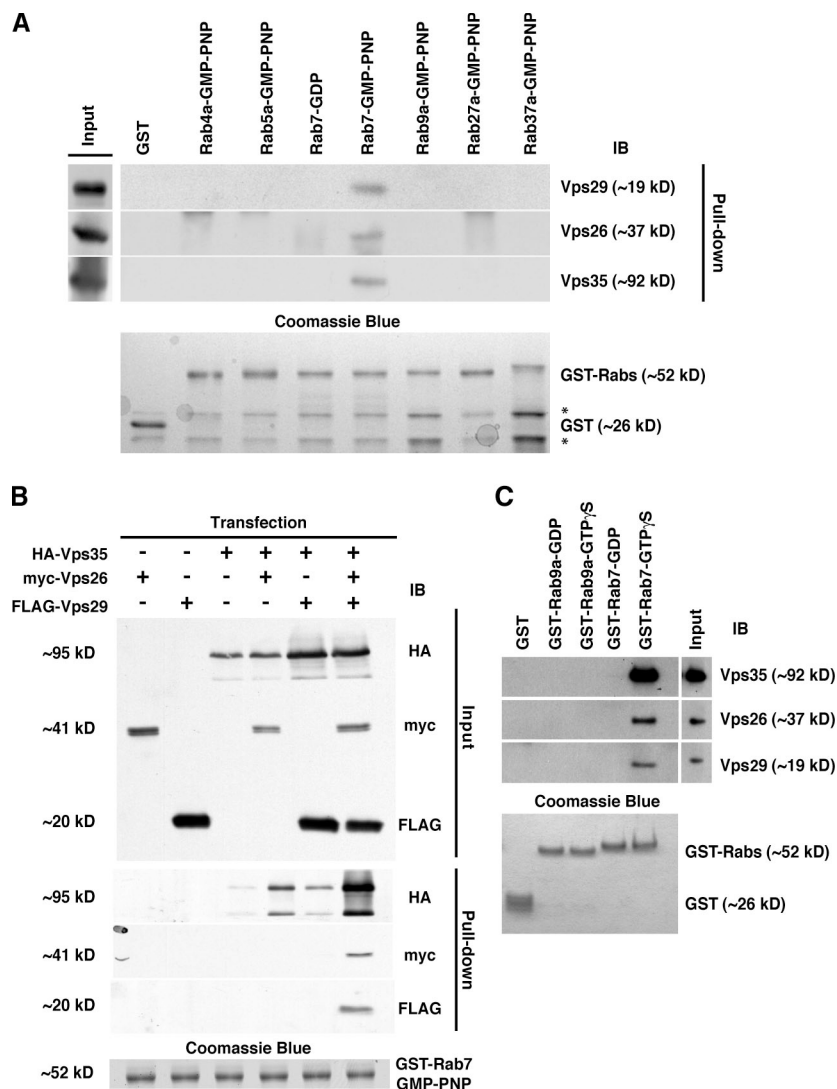
Results

Guanine nucleotide–dependent interaction of Rab7 with the retromer Vps subcomplex

In the course of studies aimed at identifying Rab effectors by affinity purification followed by mass spectrometry and/or immunoblot analysis for candidate proteins, we observed that the three subunits of the mammalian retromer Vps subcomplex, Vps26, Vps29, and Vps35, bound to GST-Rab7 in the presence of the nonhydrolyzable GTP analogue, GMP-PNP (Fig. 1 A). This binding was guanine nucleotide dependent, as it was not detected in the presence of GDP (Fig. 1 A). In addition, it was specific for Rab7 because the Vps subcomplex subunits did not bind to GST-Rab4a, -Rab5a, -Rab9a, -Rab27a, or -Rab37a, all loaded with GMP-PNP (Fig. 1 A). In contrast to the Vps subcomplex, SNX1 and SNX2 did not bind to GMP-PNP–loaded GST-Rab7 (unpublished data).

To further characterize this interaction, we performed GST pull-downs of extracts from COS-7 cells expressing different combinations of epitope-tagged forms of Vps26, Vps29, and Vps35. Small amounts of HA-Vps35 were found to bind to GST-Rab7–GMP-PNP upon expression of HA-Vps35 alone or in combination with either myc-Vps26 or FLAG-Vps29 (Fig. 1 B). However, much larger amounts of HA-Vps35, together with myc-Vps26 or FLAG-Vps29, were recovered from cells coexpressing all three subunits (Fig. 1 B). None of these species bound to GST or GST-Rab4a–GMP-PNP (unpublished data), indicating that the aforementioned pull-downs were specific. These results indicated that Vps35 might be the subunit that mediates binding to Rab7. However, optimal binding requires expression of all three subunits, probably because of a requirement of Vps subcomplex assembly for proper folding of Vps35, as previously found for the recombinant proteins (Hierro et al., 2007).

To determine whether the interaction of Rab7 with the Vps26/29/35 trimer was direct, we performed GST pull-down

A

| | Input | GST | Rab4a-GMP-PNP | Rab5a-GMP-PNP | Rab7-GDP | Rab7-GMP-PNP | Rab9a-GMP-PNP | Rab27a-GMP-PNP | Rab37a-GMP-PNP | IB |

Pull-down: Vps29 (~19 kD), Vps26 (~37 kD), Vps35 (~92 kD)

Coomassie Blue: GST-Rabs (~52 kD), GST (~26 kD)

B

Transfection

HA-Vps35	−	−	+	+	+	+
myc-Vps26	+	−	−	+	−	+
FLAG-Vps29	−	+	−	−	+	+

IB

Input: ~95 kD HA, ~41 kD myc, ~20 kD FLAG

Pull-down: ~95 kD HA, ~41 kD myc, ~20 kD FLAG

Coomassie Blue: ~52 kD GST-Rab7 GMP-PNP

C

| GST | GST-Rab9a-GDP | GST-Rab9a-GTPγS | GST-Rab7-GDP | GST-Rab7-GTPγS | Input | IB |

Vps35 (~92 kD), Vps26 (~37 kD), Vps29 (~19 kD)

Coomassie Blue: GST-Rabs (~52 kD), GST (~26 kD)

Figure 1. **Binding of the retromer Vps subcomplex to active Rab7.** (A) A Triton X-100 extract of microsomes was incubated with equivalent amounts of the indicated GST-Rab proteins preloaded with GMP-PNP or GDP. Bound proteins were eluted in Laemmli sample buffer and analyzed by SDS-PAGE and immunoblotting (IB) with antibodies to the Vps26, Vps29, or Vps35 subunits of retromer (top). The first lane represents 20% of the input. The approximate molecular masses of the different proteins are indicated in kilodaltons. Asterisks indicate contaminating proteins found in all of the GST preparations. (B) COS-7 cells were transfected with plasmids encoding myc-Vps26, FLAG-Vps29, and (HA)₃-Vps35, either individually or in the combinations indicated in the figure. Lysates from these cells were incubated with GST-Rab7-GMP-PNP–bound beads. Input and bound proteins were analyzed by SDS-PAGE and immunoblotting with antibodies to the myc, FLAG, and HA tags (top). (C) Immobilized GST, GST-Rab7, or GST-Rab9a preloaded with GDP or GTPγS was incubated with recombinant Vps26/29/35 trimer. Bound proteins were eluted and analyzed by SDS-PAGE and immunoblotting with antibodies to Vps29, Vps26, and Vps35 (top). The input represents 1.8% of the total recombinant Vps26/29/35 trimer used per reaction. The bottom panels show SDS-PAGE/Coomassie blue staining of the GST proteins used in these experiments.

assays with all purified recombinant proteins. We observed that GST-Rab7 but not GST or GST-Rab9a pulled down recombinant Vps26/29/35 trimer in the presence of another nonhydrolyzable GTP analogue, GTPγS, but not in the presence of GDP (Fig. 1 C). These findings demonstrated that the Rab7–Vps26/29/35 interaction is direct and GTP dependent, thus indicating that retromer is a true Rab7 effector.

Colocalization of Rab7 with retromer

The specific guanine nucleotide–dependent interaction of Rab7 with the retromer Vps subcomplex prompted us to examine by immunofluorescence microscopy whether these proteins colocalized within cells. Because immunostaining of HeLa cells for endogenous Rab7 gave a very weak signal, we transfected the cells with a plasmid encoding GFP-tagged Rab7. Cells were immunostained for endogenous retromer using an antibody to Vps26 and examined by confocal microscopy. Using this methodology, we observed significant colocalization (48 ± 10%, $n = 24$ cells) of endogenous Vps26 with GFP-Rab7 on vesicular structures scattered throughout the cytoplasm (Fig. 2, A–C). We also observed localization (38 ± 9%, $n = 24$ cells) of

endogenous Vps26 to GFP-Rab5a–positive structures (Fig. 2, D–F) as previously described (Arighi et al., 2004; Seaman, 2004). Similar results were obtained for the colocalization of endogenous SNX1 with GFP-Rab7 and GFP-Rab5a (unpublished data).

To assess the dynamics of association of retromer with Rab7- and Rab5-containing endosomes in live cells, we performed time-lapse fluorescence microscopy of cells transfected with plasmids encoding Vps29-YFP and either CFP-Rab7 or CFP-Rab5a (Fig. 3 and Videos 1–6, available at http://www.jcb.org/cgi/content/full/jcb.200804048/DC1). In accordance with the aforementioned immunofluorescence microscopy experiments, we visualized numerous endosomal vesicles that contained both Vps29-YFP and CFP-Rab7 (Fig. 3, A–C). Moreover, Vps29-YFP was almost always found on domains of the endosomal vesicles that also contained CFP-Rab7 (Fig. 3 B). These domains were highly dynamic and underwent aggregation and fragmentation, but Vps29-YFP remained coincident with CFP-Rab7 throughout these changes. An exception was a set of long tubules that emanated and eventually detached from the endosomes; these tubules invariably contained Vps29-YFP (Fig. 3 C, green arrows)
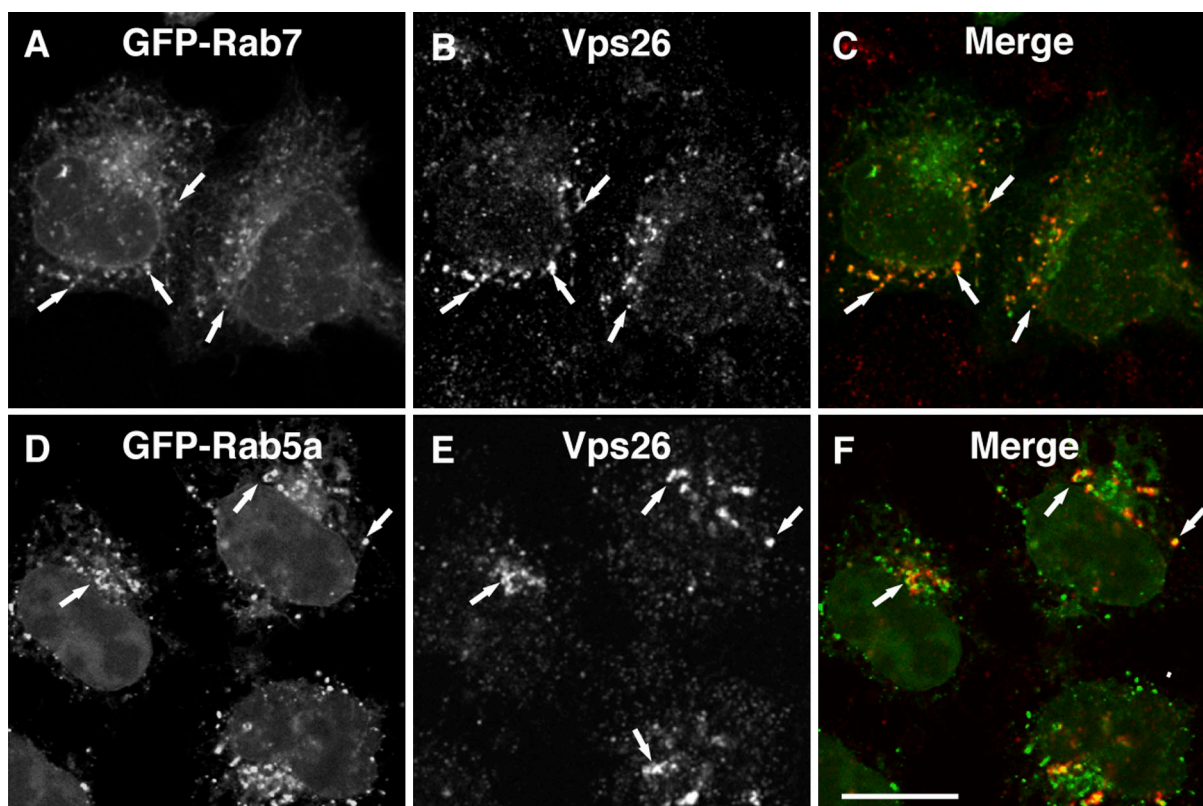
Figure 2. **Immunofluorescence microscopy showing localization of Vps26 to Rab7- and Rab5-positive endosomes.** HeLa cells were transfected with plasmids encoding GFP-Rab7 (A–C) or GFP-Rab5a (D–F), fixed, permeabilized, and immunostained with rabbit polyclonal antibody to Vps26 followed by Alexa Fluor 594–conjugated donkey anti–rabbit IgG. Cells were examined by confocal microscopy. (A and D) GFP fluorescence, green channel. (B and E) Alexa Fluor 594 fluorescence, red channel. (C and F) Merged images; yellow indicates colocalization. Arrows indicate examples of foci where proteins colocalize. Bar, 10 µm.

but not CFP-Rab7 (Fig. 3 C, red arrows). However, the tubules seemed to arise from endosomal foci where CFP-Rab7 was most concentrated (Fig. 3 C).

Vps29-YFP was also found in association with endosomal vesicles that contained CFP-Rab5a (Fig. 3, D–F). However, these two proteins were largely segregated to different domains. These domains were also highly motile and underwent changes over time, but only rarely did Vps29-YFP coincide with CFP-Rab5a (Fig. 3, D–F). Vps29-YFP–containing tubules did form from CFP-Rab5a–positive endosomes, but the tubules themselves were devoid of CFP-Rab5a (Video 4).

Although both Vps29-YFP and CFP-Rab7 decorated the limiting membrane of endosomal vesicles, they were most often concentrated within foci that appeared to bulge from the membrane (Fig. 3, A–C). To examine the ultrastructure of these foci, we performed immunoelectron microscopy. HeLa cells were transfected with a plasmid encoding GFP-Rab7 and subsequently double-immunogold labeled for endogenous Vps26 (15-nm gold) and GFP (10-nm gold; Fig. 4). Both proteins were found on multiple buds and tubules that emanated from the vacuolar part of endosomes (Fig. 4 A) and that appeared as a cluster of tubules on en face sections (Fig. 4 B). These structures are characteristic of the tubular endosomal network (Bonifacino and Rojas, 2006) that mediates retromer-dependent sorting of MPRs to the TGN, likely via the long tubules observed to extend from endosomes in the live cell imaging experiments (Fig. 3 C; Zhong et al., 2002; Arighi et al., 2004; Carlton et al., 2004, 2005b; Popoff et al., 2007).

Requirement of Rab7 for retromer association with membranes

The interaction and colocalization of Rab7 with the retromer Vps subcomplex suggested a probable functional relationship between these proteins. Rab GTPases such as Rab7 cycle between GTP-bound, membrane-associated, and GDP-bound cytosolic states and, in doing so, function to regulate the recruitment of effector proteins to membranes. To determine whether Rab7 played a role in retromer recruitment to membranes, we used RNAi to deplete Rab7 from HeLa cells (Fig. 5 A). Immunofluorescence microscopy showed that this depletion had no effect on the distribution of the adapter protein (AP) complexes AP-3 (Fig. 5 E) and AP-1 (Fig. 5 I), which are associated with specific domains of the tubular endosomal network (Futter et al., 1998; Peden et al., 2004; Theos et al., 2005), but caused virtually complete loss of endosomal staining for Vps26 (Fig. 5, D, H, L, and P). This loss was caused by dissociation from membranes and not to degradation because the levels of Vps26 protein were unchanged by depletion of Rab7 (Fig. 5 A). The effects of Rab7 depletion on Vps26 localization were specific because combined depletion of the also endosomal Rab4a and Rab4b paralogues (Fig. 5 A) did not alter the distribution of Vps26 (Fig. 6 B). Moreover, transfection of Rab7-depleted cells with a plasmid encoding an RNAi-resistant form of GFP-Rab7 (Fig. 6, C and E, arrows) but not with a plasmid encoding GFP (Fig. 6, D and F) partially restored Vps26 association with endosomes. Interestingly, SNX1 (Fig. 5 M) and SNX2 (Fig. 5 Q) retained
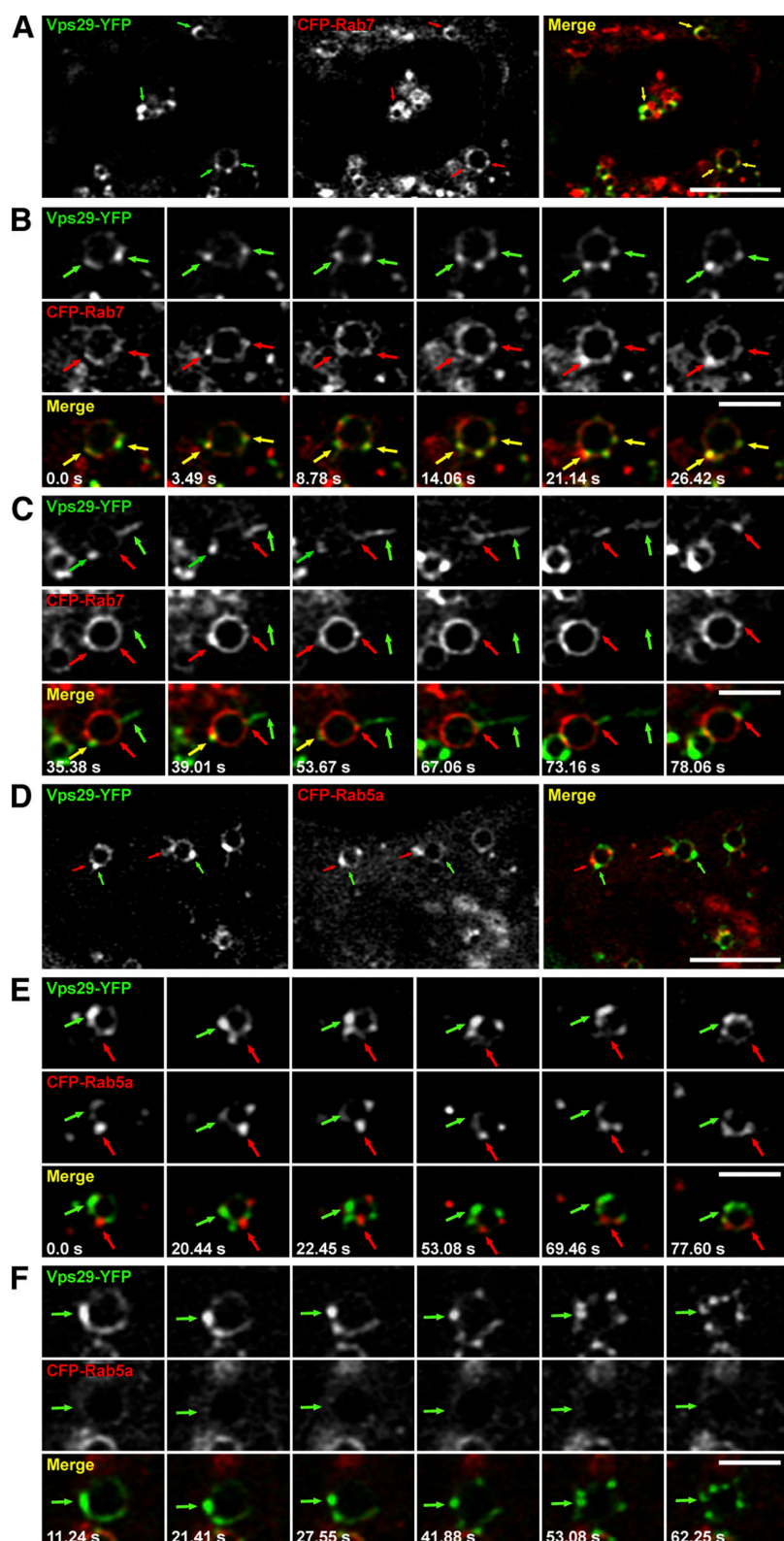
Figure 3. **Live cell imaging showing localization of Vps29-YFP to endosomal domains that contain CFP-Rab7 but not CFP-Rab5a.** HeLa cells cotransfected with plasmids encoding Vps29-YFP (green) and either CFP-Rab7 (A–C) or CFP-Rab5a (D–F; red) were imaged by time-lapse fluorescence microscopy. Pictures in this figure were extracted from Videos 1–6 (available at http://www.jcb.org/cgi/content/full/jcb.200804048/DC1). Merging the green and red images generated the third picture in A and D and the images in the bottom rows of B, C, E, and F. Yellow indicates overlapping localization of green and red objects. Examples of colocalization are indicated by yellow arrows. The images in A and the series in B and C show the localization of Vps29-YFP to domains that contain CFP-Rab7 (indicated by green and red arrows in individual channel images or yellow arrows in merge images). The series in C shows an endosome in which Vps29-YFP (green arrows) is enriched on a detaching tubule that does not contain CFP-Rab7 (red arrows). The images in D and the series in E and F show that Vps29-YFP (green arrows) and CFP-Rab5a (red arrows) are localized to different endosomal domains. The series in F shows a Vps29-YFP–positive endosome with little or no CFP-Rab5 (green arrows). Time after the start of imaging (in seconds) is shown on the bottom left corner of each panel. Bars: (A and D) 5 µm; (B, C, E, and F) 2 µm.

their association with endosomes in Rab7-depleted cells, although the endosomes appeared enlarged and more disperse. These observations highlighted another important difference in the properties of the Vps and SNX subcomplexes of retromer in that only the Vps subcomplex requires Rab7 for association with endosomes.

Dominant-negative overexpression reveals a role for Rab5 in retromer recruitment to membranes

In addition to RNAi, another commonly used approach to test for the dependence of cellular processes on small GTPases is to overexpress dominant-negative GDP-locked forms of the proteins.
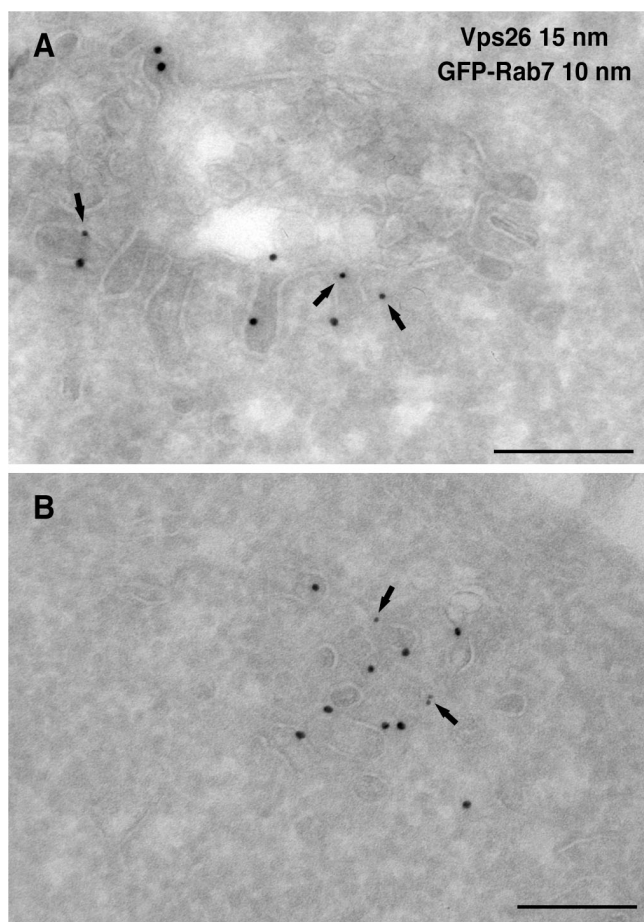
Figure 4. **Immunoelectron microscopy localization of GFP-Rab7 and Vps26.** Ultrathin cryosections of HeLa cells expressing wild-type GFP-Rab7 were immunogold labeled with antibodies to GFP (10-nm gold particles) and Vps26 (15-nm gold particles). Arrows indicate the presence of GFP-Rab7 on buds adjacent to the vacuolar part of endosomes (A) and on tubules (B). Tubules and buds are also labeled for Vps26. Bars, 200 nm.

Use of this approach showed that dominant-negative GFP-Rab7–T22N (Fig. 7 H, arrows) but not dominant-negative GFP-Rab4a–S22N (Fig. 7 B, arrows) caused dissociation of Vps26 from endosomes (to 26% of levels in control cells; Fig. S1 E, available at http://www.jcb.org/cgi/content/full/jcb.200804048/DC1). In contrast, SNX1 association with endosomes was not affected by GFP-Rab7–T22N overexpression, although the appearance of the endosomes was altered (Fig. 7 I, arrows). These results were consistent with those obtained using RNAi (Figs. 5 and 6). The dominant-negative approach was particularly useful to assess the role of Rab5 in retromer recruitment because the existence of three Rab5 paralogues (a, b, and c; Huang et al., 2004) made RNAi impractical. Surprisingly, we found that overexpression of dominant-negative GFP-Rab5a–S34N resulted in Vps26 dissociation from endosomes (to 36% of levels in control cells; Fig. 7 E, arrows; and Fig. S1 E). In striking contrast to Rab7 depletion or dominant-negative overexpression, however, dominant-negative GFP-Rab5a–S34N overexpression also caused dissociation of SNX1 from endosomes (Fig. 7 F, arrows). Because Rab5 does not interact with retromer (Fig. 1), these results probably stem from

the fact that Rab5 activates endosomal PI3K (Christoforidis et al., 1999b), which produces PI3P, an essential cofactor for SNX1 and SNX2 association with membranes (Cozier et al., 2002; Carlton et al., 2004). In turn, SNX1 and SNX2 enable the recruitment of the retromer Vps subcomplex to membranes (Rojas et al., 2007).

To analyze the interplay between PI3K and Rab7 in the regulation of retromer recruitment to membranes, we overexpressed a constitutively active GTP-locked form of Rab7 (GFP-Rab7–Q67L) and examined the effects of adding the PI3K inhibitor wortmannin. In control cells, wortmannin addition caused dissociation of both Vps26 (to 28% of levels in untreated cells) and SNX1 from membranes (Fig. 7, J–L; and Fig. S1) as previously reported (Arighi et al., 2004; Rojas et al., 2007). However, in cells overexpressing GFP-Rab7–Q67L, Vps26 (Fig. 7 K, arrows; and Fig. S1) but not SNX1 (Fig. 7 L, arrows; and Fig. S1) remained partially associated with membranes in the presence of wortmannin (76% of levels in untreated cells; Fig. S1 E). These results indicated that the nonphysiologically high level of activity of GFP-Rab7–Q67L can override the absence of PI3P for recruitment of the retromer Vps subcomplex but not the SNX subcomplex to endosomes. Thus, interaction with Rab7 and regulation by Rab5 through a PI3K–PI3P–SNX1/2 pathway cooperate to recruit the retromer Vps subcomplex to membranes.

Involvement of Rab7 in the trafficking of MPRs and their acid hydrolase cargo

Because retromer functions in the retrograde transport of the CI-MPR from endosomes to the TGN, we expected that interference with Rab7 would alter the trafficking of the receptors. Indeed, we found that the steady-state distribution of the CI-MPR changed from a juxtanuclear cluster of small vesicles (Fig. 8, A and C) to a more disperse collection of large vesicles (Fig. 8, B and D) upon depletion of Rab7 by RNAi. Incubation of control live cells with antibody to the CI-MPR at 37°C showed that the cell surface receptors were internalized and underwent retrograde transport to achieve a distribution similar to that at steady state (i.e., a mix of endosomes and TGN; Fig. 8, E and G; Seaman, 2004; Rojas et al., 2007). However, in Rab7-depleted cells, the internalized CI-MPR remained trapped in enlarged peripheral endosomes (Fig. 8, F and H). These endosomes contained the transferrin receptor (TfR; Fig. 8, I–K), identifying them as early endosomes. In contrast to retromer depletion (Arighi et al., 2004; Rojas et al., 2007), however, Rab7 depletion did not affect the levels of the CI-MPR (Fig. 8 O), indicating that the receptor was not delivered to lysosomes for degradation but accumulated in early endosomes.

The trapping of the CI-MPR in early endosomes should result in its depletion from the TGN, leading to missorting of newly synthesized acid hydrolases. Immunoblot analysis of one such hydrolase, cathepsin D, showed that this was indeed the case. In control cells, most of the cathepsin D occurred as the 31-kD mature form with only small amounts of the 53-kD precursor and 47-kD intermediate forms (Fig. 9). Only trace amounts of the precursor form were secreted into the medium in control cells (Fig. 9). This efficient processing and intracellular retention of cathepsin D reflects the integrity of the normal mechanism for trafficking of the enzyme from the TGN all the way to lysosomes. Depletion of Rab7, like depletion of Vps26 (Seaman, 2004),

A
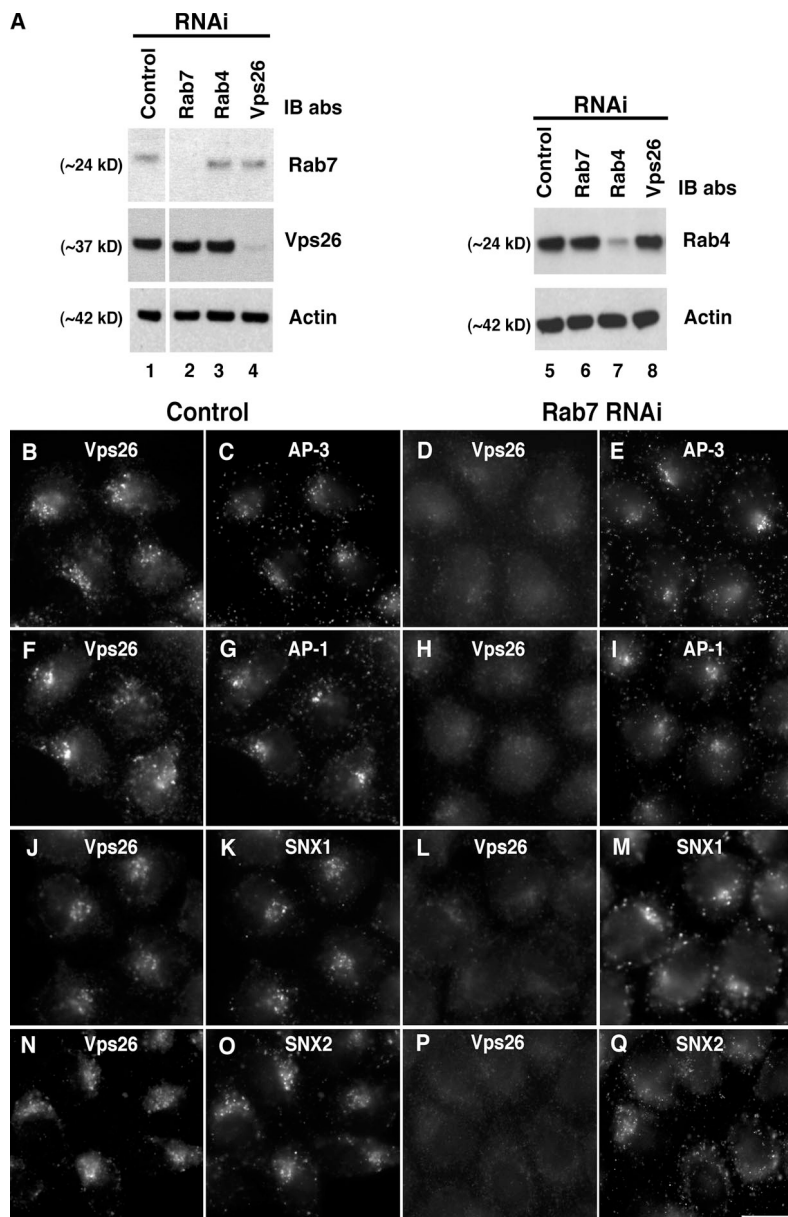
Figure 5. **RNAi-mediated depletion of Rab7 causes Vps26 dissociation from endosomes.** (A) HeLa cells were treated twice at 24-h intervals with a control, inactive siRNA, or siRNAs to Rab7, Rab4 (targeting both the a and b isoforms), or Vps26. Cell extracts were analyzed by SDS-PAGE and immunoblotting with antibodies to Rab7, Rab4, Vps26, or actin (loading control) as indicated in the figure. (B–Q) HeLa cells treated as in A with control (B, C, F, G, J, K, N, and O) or Rab7 siRNA (D, E, H, I, L, M, P, and Q) were immunostained for Vps26 (B, D, F, H, J, L, N, and P) and AP-3 (C and E), AP-1 (G and I), SNX1 (K and M), and SNX2 (O and Q) using rabbit polyclonal antibody to Vps26 and mouse monoclonal antibodies to AP-3–δ, AP-1–γ1, SNX1, or SNX2 followed by Alexa Fluor 594–conjugated donkey anti–rabbit IgG and Alexa Fluor 488–conjugated donkey anti–mouse IgG. Images were captured by epifluorescence microscopy. Bar, 10 μm.

caused substantial increases in the amount of precursor and intermediate forms present within the cells and of precursor form secreted into the medium (Fig. 9), which were indicative of impaired transport of the enzyme to lysosomes. These results are consistent with the role of Rab7 in regulating retromer function and CI-MPR sorting in endosomes.

Discussion

The results of our study indicate that Rab5 and Rab7 function in a sequential manner to regulate the recruitment of the retromer Vps subcomplex to endosomes. Rab5 does not bind the Vps subcomplex (Fig. 1), although overexpression of dominant-negative Rab5 causes dissociation of the subcomplex from endosomes (Fig. 7). In contrast, Rab7 binds retromer in a guanine nucleotide–dependent manner (Fig. 1). In addition, depletion of Rab7 by RNAi (Figs. 5 and 6) or overexpression of dominant-negative

Rab7 (Fig. 7) results in Vps subcomplex dissociation from membranes. These latter perturbations also interfere with trafficking of the CI-MPR (Fig. 8) and its cargo, cathepsin D (Fig. 9), in line with previous findings (Press et al., 1998). Thus, Rab7 constitutes the missing link in the mechanism that controls retromer recruitment to endosomes and its function in cargo sorting. These findings expand the range of processes that are known to be regulated by Rab5 and Rab7 by implicating these Rabs in retrograde transport from endosomes to the TGN.

A model for the regulation of retromer by Rab5 and Rab7

Fig. 10 depicts a model for the mechanism of recruitment of the mammalian retromer complex to endosomes based on the data presented here and in previous studies. Exchange of GTP for GDP causes Rab5 to associate with early endosomes (Ullrich et al., 1994) and to recruit a large number of effector proteins
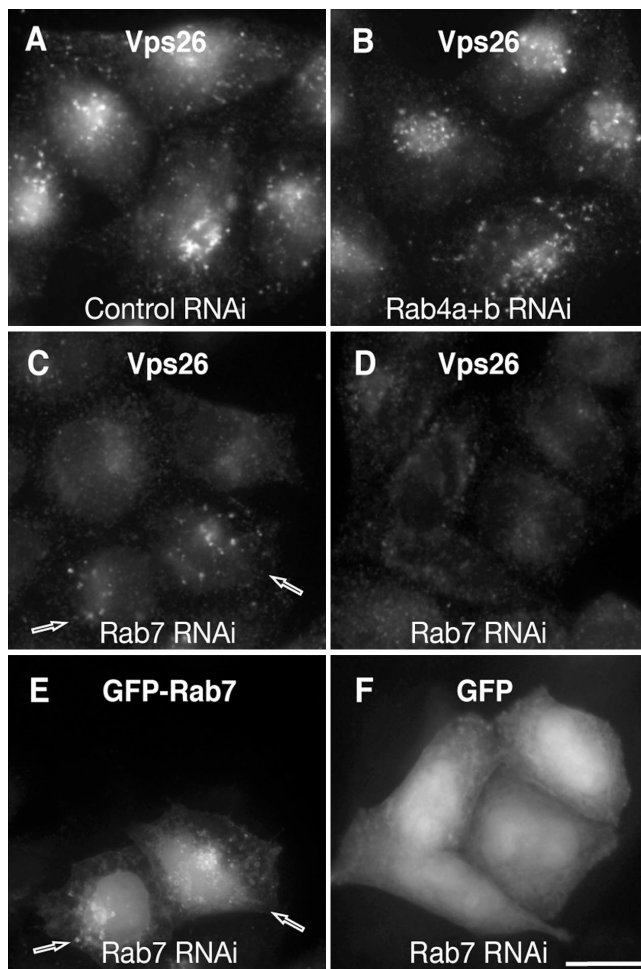
Figure 6. **Specificity and rescue of Vps26 dissociation from membranes in RNAi-treated cells.** HeLa cells were treated twice at 24-h intervals with an inactive siRNA (control; A) or siRNAs to both Rab4a and Rab4b (B) or to Rab7 (C–F). At 36 h after the second treatment with siRNA to Rab7, some cells were transfected with plasmids encoding RNAi-resistant (i.e., canine) GFP-Rab7 (C and E) or GFP (D and F). Examples of cells expressing GFP or canine GFP-Rab7 are indicated by arrows. The cellular distribution of Vps26 (A–D) was assessed by indirect immunofluorescent staining using rabbit polyclonal antibody to Vps26 followed by Alexa Fluor 594–conjugated donkey anti–rabbit IgG. Images were captured by epifluorescence microscopy. Bar, 10 µm.

(Christoforidis et al., 1999a). A key Rab5 effector is the class III PI3K (Christoforidis et al., 1999b), which in mammalian cells is composed of a catalytic Vps34 subunit and a regulatory p150 subunit (Panaretou et al., 1997). PI3K phosphorylates phosphatidylinositol to PI3P, a phosphoinositide that is highly enriched in endosomal membranes (Gillooly et al., 2000). PI3P, in turn, functions to recruit many other downstream effectors, among which are the components of the retromer SNX subcomplex (Burda et al., 2002; Cozier et al., 2002; Zhong et al., 2002, 2005; Arighi et al., 2004; Carlton et al., 2004, 2005b). These proteins bind to PI3P via their phox homology domains and to curved membranes via their Bin–Amphiphysin–Rvs domains in a process that is referred to as coincidence detection (Carlton et al., 2004; Carlton and Cullen, 2005). The SNX subcomplex contributes to the recruitment of the Vps subcomplex probably by virtue of interactions between the largely unstructured

N-terminal extensions (Gullapalli et al., 2004) and several binding sites on the Vps29 and Vps35 subunits (Collins et al., 2005). However, these interactions are too weak to fully account for the association of the Vps subcomplex with endosomes (Rojas et al., 2007). That is where Rab7 comes into play. Another Rab5 effector is the homotypic fusion and vacuole protein sorting–Vps-C complex, which functions as a Rab7 guanine nucleotide exchange factor (Rink et al., 2005). Activation of Rab7 by exchange of GTP for GDP results in binding of Rab7-GTP to membranes, thus providing an additional attachment point for the Vps subcomplex to associate with endosomes. This cooperation of the SNX subcomplex and Rab7 represents another layer of coincidence detection that further specifies the recruitment of the Vps subcomplex to particular endosomal domains. Rab7 also interacts with and activates PI3K (Stein et al., 2003), ensuring sustained production of PI3P for SNX subcomplex recruitment after dissociation of Rab5 from endosomes. The relative contributions of the SNX proteins and Rab7 to Vps subcomplex recruitment vary in other organisms. In the yeast *Saccharomyces cerevisiae*, the two SNX1/2 orthologues, Vps5p and Vps17p, are much more tightly associated with the corresponding Vps subcomplex subunits, to the point that all five subunits can be coprecipitated from cell extracts (Seaman et al., 1998; Gokool et al., 2007). At the other end of the range is *Entamoeba histolytica*, which has a Vps subcomplex that interacts with Rab7 but apparently has no SNX-like proteins encoded in its genome (Nakada-Tsukui et al., 2005). The interaction of *E. histolytica* Rab7 with the Vps subcomplex has another feature that appears unique to this organism in that Rab7 binding requires the long C-terminal extension of Vps26 that is not present in the mammalian and yeast orthologues (Nakada-Tsukui et al., 2005). This is in contrast to the interaction of the mammalian proteins, which involves binding of Rab7 to the fully assembled Vps subcomplex probably through direct contact with Vps35 (Fig. 1 B).

Endosomal domains involved in retromer function

The aforementioned steps take place as the endosomes undergo the process of Rab conversion (Rink et al., 2005), in which Rab5 is replaced by Rab7 during endosomal maturation. Rab5 is associated with the plasma membrane (Sato et al., 2005) and early endosomes (Chavrier et al., 1990). It is at this early endosomal stage that PI3K starts producing PI3P and that the SNX subcomplex can be first recruited to endosomes. Only during the brief interval when Rab5 is being replaced by Rab7 do both Rabs coexist on the same endosome (Rink et al., 2005; Vonderheit and Helenius, 2005). The arrival of Rab7 completes the set of regulators needed for recruitment of the Vps subcomplex to membranes. Upon dissociation of Rab5, Rab7 assumes complete control of Vps subcomplex recruitment via continued activation of the PI3K–PI3P–SNX pathway and direct interaction with the Vps subcomplex (Fig. 10). This coincidence of events regulated by Rab7 accounts for the predominant localization of the Vps subcomplex to Rab7 domains (Fig. 3 and Videos 1–6). All of these events occur while the proteins are associated with the vacuolar aspect of the endosomes. However, both Rab7 and retromer are
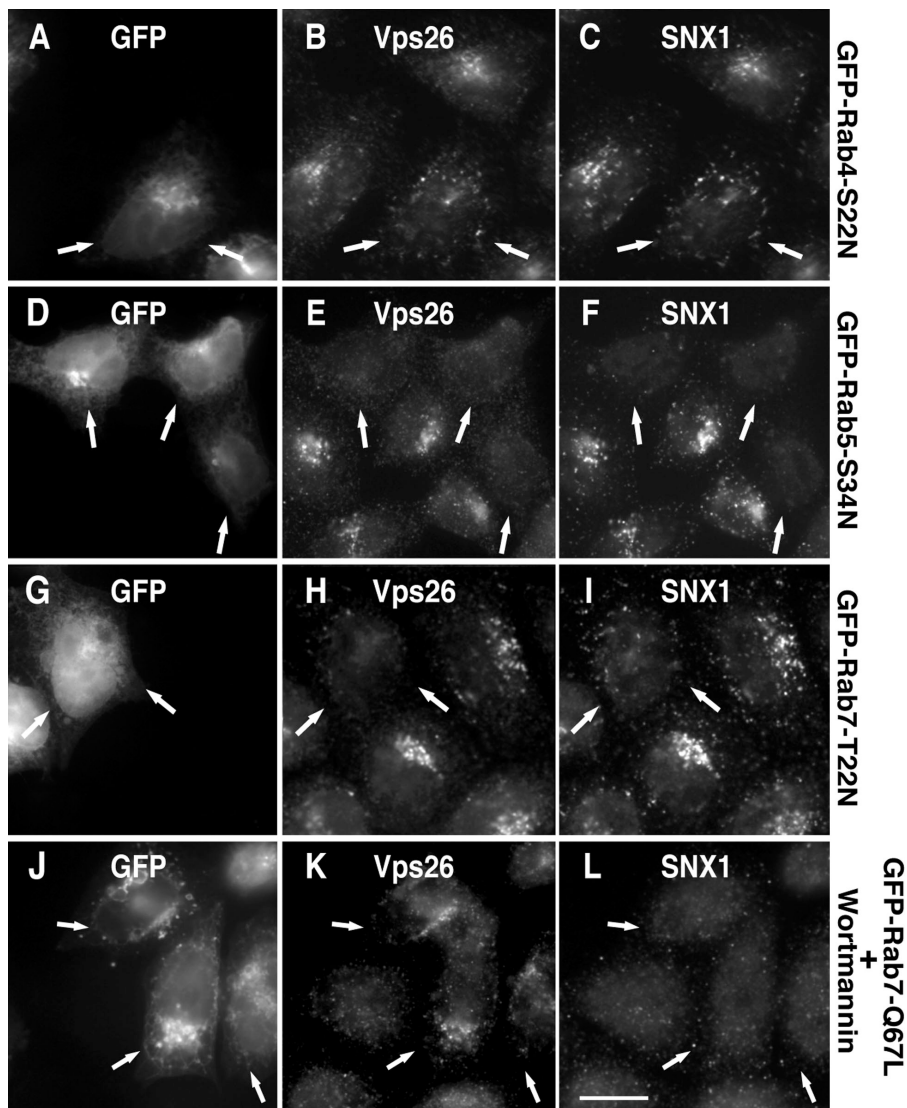
Figure 7. **Dominant-negative forms of Rab5 or Rab7 alter the association of retromer with endosomes.** (A–I) HeLa cells were transfected with plasmids encoding GFP-Rab4a–S22N (A–C), GFP-Rab5a–S34N (D–F), GFP-Rab7–T22N (G–I), or GFP-Rab7–Q67L. At 8 h after transfection, the cellular distribution of Vps26 (B, E, and H) and SNX1 (C, F, and I) was analyzed by indirect immunofluorescent staining using rabbit polyclonal antibody to Vps26 and mouse monoclonal antibodies to SNX1 followed by Alexa Fluor 594–conjugated donkey anti–rabbit IgG and Alexa Fluor 647–conjugated donkey anti–mouse IgG. (J–L) Cells were treated with 200 nM wortmannin in DMSO for 30 min at 37°C and the distribution of Vps26 and SNX1 was analyzed by indirect immunofluorescent staining using the respective primary antibodies and fluorescently labelled secondary antibodies. Images were captured by epifluorescence microscopy. Arrows point to cells expressing the GFP-Rabs. Bar, 10 µm.

also found on a convoluted set of buds and tubules adjacent to the vacuolar aspect of endosomes (Fig. 4). At some point, both the SNX and Vps subcomplexes of retromer begin to leave the endosomes on long tubular extensions that eventually detach (Fig. 3 C and Videos 3 and 4). A population of endosome to TGN carriers has also been shown to form from such sites (Mari et al., 2008). This process probably starts at the stage of the transitional Rab5–Rab7 endosomes, as some retromer-containing tubules can be seen to emanate from Rab5-positive endosomes (Video 4). However, conversion to Rab7 status brings about an intensification of retromer–tubule formation. Remarkably, Rab7 does not accompany retromer into the long tubules (Fig. 3 C and Video 3), suggesting that the stabilizing role of Rab7 must be taken over by some other factor. This role is likely fulfilled by cargo proteins such as the CI-MPR, as is the case for other cargo–adapter interactions (Fig. 10; Hirst et al., 2007).

Rab7 as a master regulator of multiple endosomal processes

Rab7 has several other effectors in addition to retromer and homotypic fusion and vacuole protein sorting–Vps-C. Among these are Rab-interacting lysosomal protein (Cantalupo et al., 2001) and ORP1L (Johansson et al., 2005), which form a complex that interacts with dynein–dynactin motors to effect minus end–directed tracking of late endosomes on microtubules (Johansson et al., 2007). Another Rab7 effector is Rabring7, an ubiquitin ligase that promotes targeting of internalized EGF receptors for lysosomal degradation (Sakane et al., 2007). Notably, all of these effectors other than retromer are known to mediate processes that take place in the vacuolar part of late endosomes and that lead to lysosomes. Thus, our findings uncover a new role for Rab7 in controlling an essentially distinct process, the diversion of cargo away from lysosomes and into recycling tubules. Not only does Rab7 control this retrograde transport pathway, but it can actually be found on a tubular network adjacent to endosomes (Fig. 4). Thus, Rab7 acts as a master control switch that regulates multiple endosomal processes. Along these lines, Rab7 has been recently shown to modulate retrograde axonal transport of vesicles containing neurotrophins and their receptors in motor neurons (Deinhardt et al., 2006). It is perhaps because of the involvement of Rab7 in protein transport

Figure 8. **Depletion of Rab7 blocks the transport of CI-MPR from endosomes to the TGN.** HeLa cells were treated twice at 24-h intervals with an inactive siRNA (control; A, C, E, and G) or siRNA to Rab7 (B, D, F, and H–N). At 48 h after treatment, the steady-state distribution of CI-MPR (A–D) was assessed by indirect immunofluorescent staining of fixed cells using rabbit polyclonal antibody to cytosolic tail of CI-MPR followed by Alexa Fluor 488–conjugated donkey anti–rabbit IgG. C and D correspond to high magnification views of CI-MPR–positive structures from control or Rab7-depleted cells, respectively. Live control cells (E and G) or Rab7-depleted cells (F and H–N) were incubated with an antibody to the luminal domain of CI-MPR for 2 h at 37°C. Cells were washed, fixed, permeabilized, and stained with Alexa Fluor 488–conjugated donkey anti–mouse IgG to detect internalized antibody to CI-MPR (E–H, J, and M). G and H show high magnification views from control (E) or Rab7-depleted cells (F), respectively. Cells in I–N were additionally stained with rabbit polyclonal antibody to TfR (I–K) or giantin (L–N) followed by Alexa Fluor 594–conjugated donkey anti–rabbit IgG. Images in A–H were captured using an epifluorescence microscope, and images in I–N were captured with a confocal microscope. (K and N) For merged images, yellow indicates colocalization. Arrows in I–K indicate examples of foci where proteins colocalize. (O) Extracts of HeLa cells treated with siRNAs to the proteins indicated on top were analyzed by 4–20% acrylamide gradient SDS-PAGE and immunoblotting (IB) with antibodies to the proteins indicated on the right. Equal amounts of total protein were loaded. Bars: (A, B, E, and F) 15 μm; (C, D, G, and H) 1.5 μm; (I–N) 10 μm.
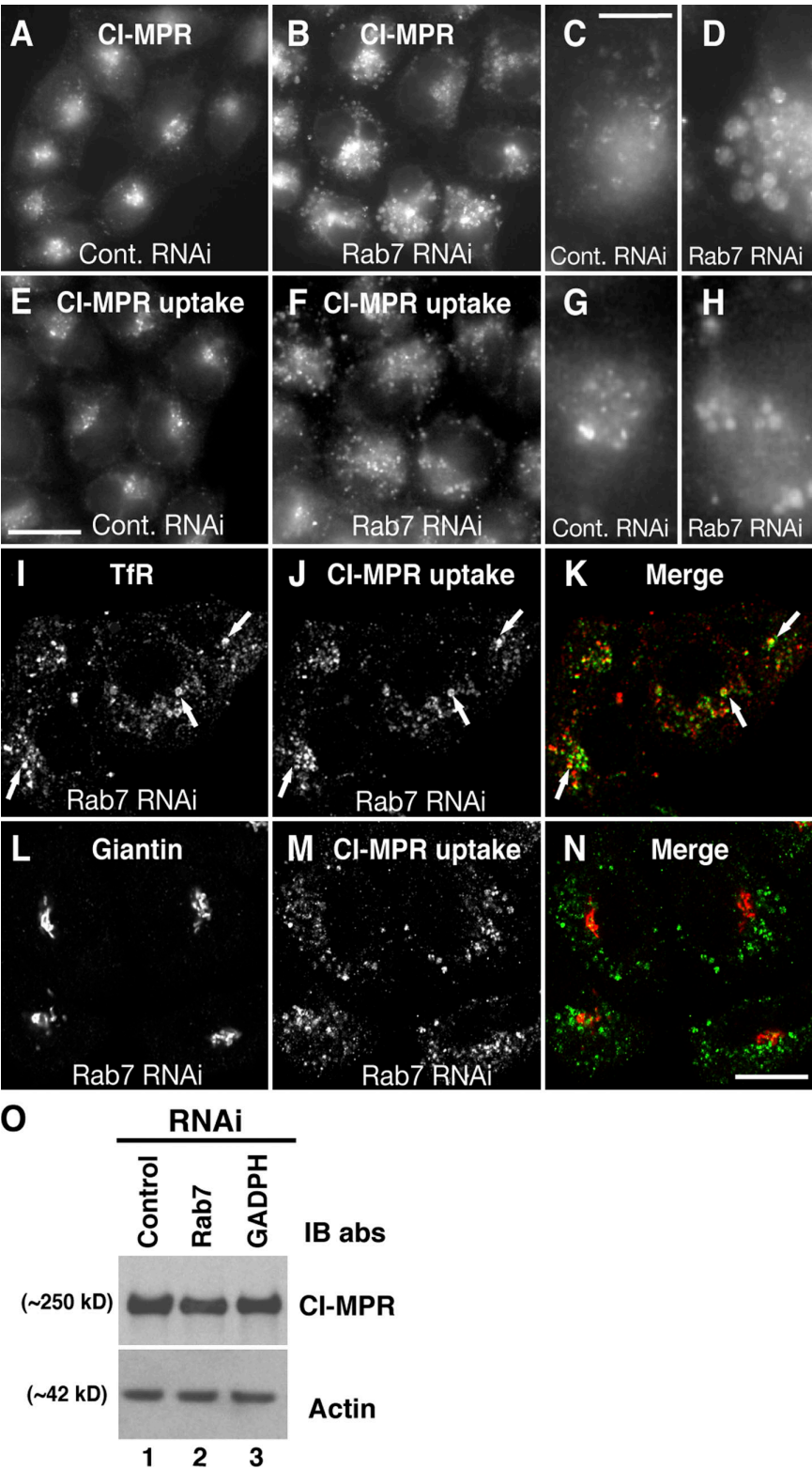
pathways that lead both toward and away from lysosomes that interference with Rab7 function does not result in targeting of the CI-MPR to lysosomes, as is the case for retromer depletion (Arighi et al., 2004; Carlton et al., 2004; Seaman, 2004; Rojas et al., 2007), but in its accumulation in endosomes (Fig. 8).

Endosomal sites of retrieval to the TGN

The retrieval of unoccupied CI-MPR to the TGN was long thought to occur from late endosomes. Indeed, an ensemble of the late endosomal Rab9 and its effector TIP47 were shown to play a role in this process (Carroll et al., 2001). However, there was also evidence that at least some retrieval took place from early
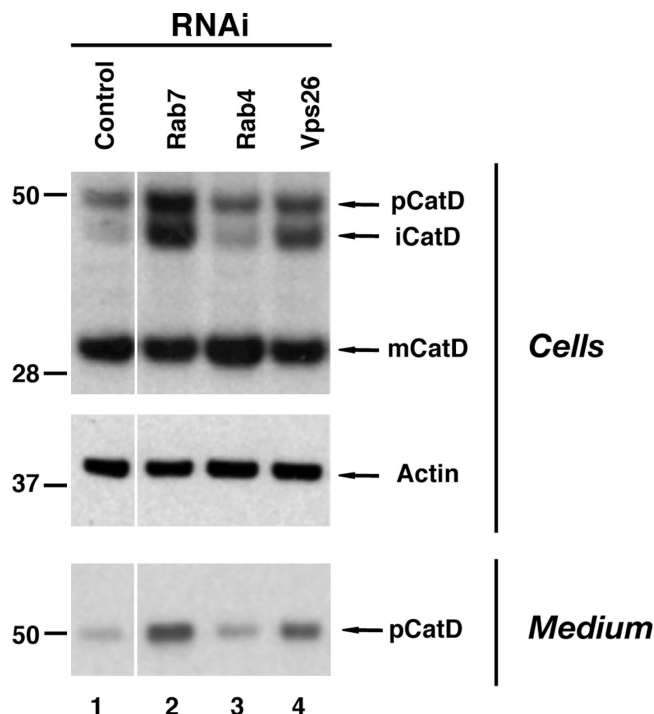
Figure 9. Rab7 depletion impairs processing of cathepsin D. HeLa cells were treated twice at 24-h intervals with inactive siRNA (control; lane 1) or siRNAs to the proteins indicated on top. At 24 h after the second round of siRNA treatment, cells were rinsed with PBS and incubated in serum-free culture medium for 24 h. The medium was collected and precipitated with trichloroacetic acid, and the resulting pellets were dissolved in Laemmli sample buffer. Cell extracts and media samples were analyzed by 4–20% acrylamide gradient SDS-PAGE and immunoblotting with rabbit polyclonal antibody to cathepsin D. Equal amounts of total protein were loaded on each lane. Blots were also probed with antibody to actin as a loading control. The positions of molecular mass markers (in kilodaltons) and of the precursor (pCatD), intermediate (iCatD), and mature (mCatD) forms of cathepsin D are indicated.

endosomes (Press et al., 1998). This latter view was bolstered by the demonstration that the mammalian retromer, which mediates CI-MPR retrieval, is associated with a population of endosomes that have the morphological features of intermediates in the maturation from early to late endosomes (Arighi et al., 2004; Carlton et al., 2004; Seaman, 2004; Bujny et al., 2007; Popoff et al., 2007). This is consistent with the finding that some retromer localizes to Rab5-positive endosomes (Figs. 2 and 3 and Videos 4–6; Gullapalli et al., 2004). Even the *S. cerevisiae* retromer is now believed to localize to tubular elements, some of which may be derived from early endosomes (Strochlic et al., 2007). It thus appears that CI-MPR retrieval occurs from a continuum of maturing endosomes that starts in early endosomes through a Rab7–retromer pathway and ends in late endosomes through a Rab9–TIP47 pathway.

Materials and methods

Recombinant DNA procedures

The construction of GST-Rab4a, GST-Rab5a, GST-Rab7, and GST-Rab27a was described previously (Neeft et al., 2005). A GST-Rab9a construct was provided by S. Pfeffer (Stanford University, Stanford, CA). A Rab37a cDNA was obtained from E. Masuda (Rigel Inc., San Francisco, CA) and ligated in frame into the BamHI and EcoRI sites of pGEX1λT. A GFP-Rab5a con-

struct was generated by in-frame cloning of canine Rab5a cDNA (provided by M. Zerial, Max Planck Institute, Dresden, Germany) into the KpnI and BamHI sites of the pEGFP-C1 vector (BD Biosciences). Complementary DNAs encoding Rab7 and Rab4a were amplified by PCR from a canine cDNA library and cloned in frame into the KpnI–ApaI and BglII–KpnI sites, respectively, of the pEGFP-C1 vector. The QuikChange Site-Directed Mutagenesis kit (Stratagene) was used to produce the following mutants: GFP-Rab4a–S22N, GFP-Rab5a–S34N, GFP-Rab7–T22N, and GFP-Rab7–Q67L. The CFP-Rab5a construct was generated as previously described (Sonnichsen et al., 2000). The Vps29-YFP construct was generated by PCR amplification of human Vps29 (residues 1–182; the stop codon TAA at position 183 was mutated to TAT, encoding a tyrosine residue) and cloning into the EcoRI and BamHI sites of the pEYFP-N1 vector (BD Biosciences). The pEF-BOS-FLAG-Vps29 construct was obtained by PCR amplification of full-length human Vps29 cDNA from a previously described pcDNA3.1-Vps29-myc construct and cloned into the NotI (at both 5′ and 3′ ends) site of the pEF-BOS vector. Full-length human Vps26 cDNA was cloned in frame into the BamHI and EcoRI sites of the pRK5myc vector. (HA)₃-Vps35-pEF6/V5 has been described previously (Hierro et al., 2007).

GST affinity purification and pull-down experiments

A membrane extract was prepared by homogenizing 100 g of pig kidney in 1 vol of 20 mM Hepes, pH 7.5, 100 mM NaCl, 5 mM MgCl$_2$, and 1 mM DTT (buffer A) supplemented with 10 μg/ml DNase, 10 μg/ml RNase, 1 mM PMSF, 10 μg/ml aprotinin, 1 μg/ml pepstatin, and 5 μg/ml leupeptin at 4°C. Insoluble material was removed by centrifugation at 20,000 g. The supernatant was recentrifuged for 1 h at 100,000 g to collect a membrane fraction. The pellet was resuspended in 10 ml of buffer A containing 1% (wt/vol) Triton X-100 and extracted for 30 min on ice. The extract was diluted fivefold with buffer A and dialyzed overnight against 5 mM MgCl$_2$, 1 mM DTT, and 0.2% (wt/vol) Triton X-100 in PBS. The extract was recentrifuged at 100,000 g and used for binding assays. GST-Rab fusion proteins were produced in *Escherichia coli* BL21(DE3)-CodonPlus-RIL (Stratagene). The details of this purification have been described previously (Neeft et al., 2005). Guanine nucleotide exchange on immobilized GST-Rab proteins was performed as previously described (Christoforidis and Zerial, 2000; Neeft et al., 2005). Immobilized GST-Rab proteins loaded with GMP-PNP or GDP were incubated with the kidney membrane extract at 4°C by end over end rotation. After 2 h, the beads were washed four times with 1 ml of buffer A containing 20 μM GMP-PNP or GDP, twice with 1 ml of buffer A supplemented with the appropriate nucleotide and 250 mM NaCl, and finally twice with 1 ml of 20 mM Hepes, pH 7.5, 250 mM NaCl, and 1 mM DTT. Bound proteins were analyzed by SDS-PAGE and immunoblotting.

For pull-down experiments, we transfected individually or together pRK5-myc-Vps26, pEF-BOS-FLAG-Vps29, and pEF-HA-Vps35 in COS-7 cells using Lipofectamine-2000 (Invitrogen). After 24 h, the cells were washed with ice-cold PBS and lysed in 20 mM Hepes, pH 7.5, 100 mM NaCl, 5 mM MgCl$_2$, and 0.2% (wt/vol) NP-40 for 10 min on ice. Lysates were spun for 10 min at 15,700 g in a benchtop centrifuge (Eppendorf). Supernatants were collected and later incubated with GST-Rab7–GMP-PNP (or GST or GST-Rab4a–GMP-PNP as negative controls) bound to glutathione–agarose beads for 2 h in an end over end device. Samples were subsequently washed six times with lysis buffer, the excess buffer was drained with a 30.5-gauge needle, and bound proteins were eluted by boiling in Laemmli sample buffer. Samples were analyzed by SDS-PAGE and immunoblotting with rabbit polyclonal antibodies to the myc, FLAG, and HA tags.

For in vitro binding experiments with purified recombinant proteins, GST-Rab7 and GST-Rab9a were produced in *E. coli* BL21(DE3) using ZYM-5052 autoinduction medium at 25°C (the C-terminal 23 amino acid residues from Rab9a were removed for better yields). GST-Rab proteins were immobilized on glutathione–Sepharose 4B beads, eluted according to the manufacturer's instructions, concentrated with a centrifugal concentrator (Amicon-15; Millipore), and purified on a Superdex 200 16/60 gel filtration column. For pull-down assays, 60 nmol of each GST-Rab was immobilized by incubation with 40 μl glutathione–Sepharose 4B beads in PBS, 5 mM MgCl$_2$, 1 mM DTT, 0.1% (wt/vol) NP-40, and 20 μM GDP. 300 nmol recombinant Vps35/26/29 trimer, which was produced and purified as described previously (Hierro et al., 2007), was incubated in buffer A containing 0.05% (wt/vol) BSA and 100 μM of the respective nucleotide with 60 nmol immobilized GST, GST-Rab7, or GST-Rab9a loaded with GDP or GTPγS as described previously (Christoforidis and Zerial, 2000) in an end over end rotation device at 4°C. After 2 h, samples were washed twice with buffer A with 100 μM of the respective nucleotide, twice with buffer A containing 250 mM NaCl and 100 μM of the respective nucleotide, and once with 20 mM Hepes, pH 7.5, 250 mM NaCl, 1 mM DTT, and 100 μM of the respective nucleotide. Bound retromer was eluted with 20 mM
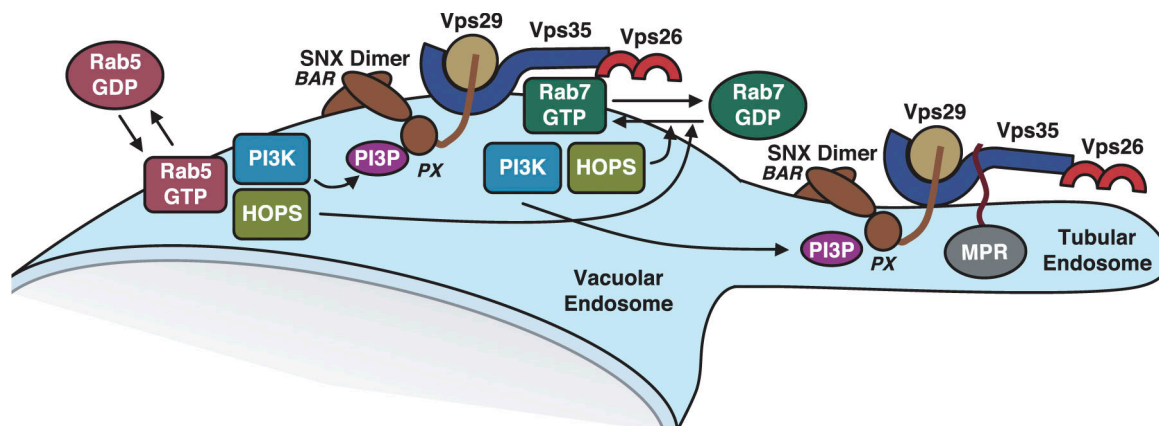
Figure 10. **Schematic representation of the regulation of retromer by Rab5 and Rab7.** The scheme depicts a section of an endosome with its vacuolar and tubular aspects. The sequence of reactions is represented in the context of the progression from Rab5- to Rab7-positive endosomes and from the vacuolar to the tubular aspect. Details of this model are described in the Discussion section. BAR, Bin–Amphiphysin–Rvs; HOPS, homotypic fusion and vacuole protein sorting; PX, phox homology.

Hepes, pH 7.5, 1.5 M NaCl, 20 mM EDTA, 1 mM DTT, and 5 mM of each nucleotide (GDP for proteins bound to the GTPγS-loaded GST-Rab and vice versa). Eluates were mixed with an equal volume of NuPAGE sample buffer and processed for SDS-PAGE and immunoblotting.

Antibodies
We used mouse monoclonal antibodies to the following proteins: Rab4, SNX1, SNX2, AP-1–γ1, and actin (BD Biosciences), CI-MPR (luminal domain; AbD Serotec), and AP-3–δ (SA4; Developmental Studies Hybridoma Bank). We also used rabbit polyclonal antibodies to the following proteins: Rab7 (provided by G. Schiavo, Cancer Research UK, London, UK; Deinhardt et al., 2006), CI-MPR cytosolic tail (Kametaka et al., 2005), Vps26, Vps29, and Vps35 (provided by C.R. Haft, National Institutes of Health, Bethesda, MD; Haft et al., 2000), cathepsin D (EMD), GFP (Invitrogen), giantin (Covance), and TfR (Millipore). A goat antibody to the Vps29 peptide DDVKVRIEYKKD was obtained from Genetex, Inc. Polyclonal antibodies to the myc and FLAG tags were obtained from Sigma-Aldrich, and the HA antibody was obtained from Upstate Cell Signaling. Donkey anti–mouse IgG conjugated to Alexa Fluor 488, donkey anti–rabbit IgG conjugated to Alexa Fluor 594, and donkey anti–mouse IgG conjugated to Alexa Fluor 647 were purchased from Invitrogen. Horseradish peroxidase–conjugated anti–mouse and anti–rabbit IgG were purchased from GE Healthcare.

Cell transfection, immunofluorescence microscopy, and quantitative analyses
For expression of GFP-tagged proteins, HeLa cells (American Type Culture Collection) grown on coverslips to 50% confluency were transfected in 24-well plates with 0.8 µg of plasmids encoding GFP, GFP-Rab7, GFP-Rab5a, GFP-Rab7–Q67L, GFP-Rab4a–S22N, GFP-Rab5a–S34N, or GFP-Rab7–T22N using Lipofectamine-2000. In some experiments, control cells or cells expressing GFP-Rab7–Q67L were incubated with 0.1% DMSO or 200 nM wortmannin in DMSO for 30 min. Cells were fixed, permeabilized, and immunostained with rabbit polyclonal antibody to Vps26 followed by Alexa Fluor 594–conjugated donkey anti–rabbit IgG. For CI-MPR antibody uptake assays, cells were rinsed twice with MEM/BSA and incubated with mouse monoclonal antibody to the luminal domain of 10 µg/ml CI-MPR in MEM/BSA for 2 h at 37°C (Rojas et al., 2007). Procedures for immunofluorescent staining of fixed and permeabilized cells were performed as previously described (Rojas et al., 2007).

Colocalization images shown in Fig. 2 and Fig. 8 (I–N) were obtained using a confocal microscope (TCS SP-2; Leica) equipped with 488-nm Ar–Kr, 543/594-nm He–Ne, and 633-nm He–Ne lasers. Images were acquired in a sequential mode using a 63× Plan Apochrom NA 1.4 oil objective and the appropriate filter combination. Settings used were as follows: photomultipliers at 400–700 V, Airy = 1, zoom = 3–4, and Kalman filter ($n = 4$). Images shown in Figs. 5–7 and 8 (A–G) were obtained with an epifluorescence microscope (AX10; Carl Zeiss, Inc.) with a Plan Apochromat 63× NA 1.3 oil objective equipped with a charge-coupled device camera (AxioCamMRm; Carl Zeiss, Inc.). All images were saved as TIFF files, contrast was adjusted with Photoshop (version 7.0; Adobe), and images were imported into Illustrator (CS; Adobe).

For quantification of Vps26 colocalization with GFP-Rab7 or GFP-Rab5a, each set of images was corrected for cross talk. We captured 512 × 512-pixel (voxel width and height, 100–150 nm; voxel depth, 250–300 nm) confocal sections (8 bit) through the whole volume of 24 cells. After image thresholding, the extent of colocalization was obtained by calculating the Manders' coefficients (M_1) and the corresponding standard deviation (Bolte and Cordelieres, 2006) with the intensity correlation analysis plug in developed for the ImageJ 1.36b software (National Institutes of Health). The percentage of colocalization was obtained by multiplying M_1 by 100.

To quantify cytosolic and membrane-bound levels of Vps26, we measured the mean total fluorescent intensity from DMSO-treated cells, GFP-Rab5aS34N–transfected cells, GFP-Rab7–T22N-transfected-cells, and untransfected or GFP-Rab7–Q67L-transfected cells treated with wortmannin. We took advantage of the fact that endogenous cytosolic proteins but not membrane-bound proteins are partially extracted on immunofluorescent staining of fixed permeabilized cells (Reinacher-Schick and Gumbiner, 2001). Therefore, we captured 512 × 512-pixel confocal (8 bit) sections through the whole volume of the cells. Using ImageJ 1.36b software, we obtained 32-bit stacks from the individual confocal sections. We measured the mean total fluorescence intensity per cell surface area and the corresponding standard deviation of the cellular Vps26 fluorescence signal of at least 25 individual cells for each condition.

Time-lapse fluorescence microscopy
HeLa cells grown to 40–50% confluency on 35-mm glass-bottom culture dishes (MatTek Corporation) were transfected with a plasmid encoding Vps29-YFP. 24 h after transfection, cells were transfected with plasmids encoding either CFP-Rab5a or CFP-Rab7. Transfections were made using Lipofectamine-2000. 12 h after the second round of transfection, cells were imaged as described previously (Mardones et al., 2007). In brief, the culture medium was replaced with phenol red–free Hepes-buffered medium (Invitrogen), and cells were kept at 37°C by using a stage incubator (ASI 400 Air Stream; Nevtek). Time-lapse fluorescence images were acquired with a confocal scanner (Ultraview; PerkinElmer) on an inverted microscope (Eclipse TE2000-S; Nikon) equipped with a PlanApo 100× NA 1.40 oil immersion objective (Nikon) and a 12-bit charge-coupled device camera (ORCA; Hamamatsu Photonics). Image capture and data acquisition were performed using Ultraview LCI software (PerkinElmer). Images were acquired in binning 2 × 2 modes to increase the signal to noise ratio at 0.25–1-s intervals. Sequence images were exported as single TIFF files, and Quicktime videos were produced using ImageJ 1.36b. To prepare figures, single frames were processed with Photoshop (version 7.0).

Electron microscopy
HeLa cells transfected with GFP-Rab7 were fixed with 2% (wt/vol) paraformaldehyde or a mixture of 2% (wt/vol) paraformaldehyde and 0.2% (wt/vol) glutaraldehyde in 0.1 M sodium phosphate buffer, pH 7.4. Cell pellets were processed for ultracryomicrotomy as described previously (Raposo et al., 1997). Ultrathin cryosections were single- or double-immunogold labeled with the indicated antibodies and using protein A conjugated to 10- or 15-nm gold particles (Cell Microscopy Center, Utrecht Medical School).

Sections were analyzed under an electron microscope (Philips CM120; FEI), and digital acquisitions were made with a numeric camera (Keen View; Soft Imaging System).

RNAi
HeLa cells grown to 30% confluency were transfected twice at 24-h intervals with 80 pmol siRNA oligonucleotides (SMARTpool reagents to Vps26, Rab7, Rab4a, Rab4b, and glyceraldehyde 3-phosphate dehydrogenase [control]; Thermo Fisher Scientific) using Oligofectamine (Invitrogen). For most experiments, cells were analyzed 48 h after the second round of transfection. In rescue experiments, cDNA encoding canine GFP-Rab7 or GFP alone were transfected using Lipofectamine-2000 into Rab7-depleted cells 36 h after the second siRNA treatment. At 12 h after transfection, cells were fixed and processed for immunofluorescence microscopy.

Other procedures
Cathepsin D processing and secretion assays, SDS-PAGE, and immunoblotting were performed as previously described (Mardones et al., 2007).

Online supplemental material
Fig. S1 shows wortmannin effects on retromer association with membranes. Videos 1–6 are time-lapse experiments of HeLa cells cotransfected with plasmids encoding Vps29-YFP and either CFP-Rab5a (Videos 1–3) or CFP-Rab7 (Videos 4–6), as described in Materials and methods. Online supplemental material is available at http://www.jcb.org/cgi/content/full/jcb.200804048/DC1.

References

Arighi, C.N., L.M. Hartnell, R.C. Aguilar, C.R. Haft, and J.S. Bonifacino. 2004. Role of the mammalian retromer in sorting of the cation-independent mannose 6-phosphate receptor. *J. Cell Biol.* 165:123–133.

Bolte, S., and F.P. Cordelieres. 2006. A guided tour into subcellular colocalization analysis in light microscopy. *J. Microsc.* 224:213–232.

Bonifacino, J.S., and J.H. Hurley. 2008. Retromer. *Curr. Opin. Cell Biol.* 20:427–436.

Bonifacino, J.S., and R. Rojas. 2006. Retrograde transport from endosomes to the trans-Golgi network. *Nat. Rev. Mol. Cell Biol.* 7:568–579.

Bujny, M.V., V. Popoff, L. Johannes, and P.J. Cullen. 2007. The retromer component sorting nexin-1 is required for efficient retrograde transport of Shiga toxin from early endosome to the trans Golgi network. *J. Cell Sci.* 120:2010–2021.

Burda, P., S.M. Padilla, S. Sarkar, and S.D. Emr. 2002. Retromer function in endosome-to-Golgi retrograde transport is regulated by the yeast Vps34 PtdIns 3-kinase. *J. Cell Sci.* 115:3889–3900.

Cantalupo, G., P. Alifano, V. Roberti, C.B. Bruni, and C. Bucci. 2001. Rab-interacting lysosomal protein (RILP): the Rab7 effector required for transport to lysosomes. *EMBO J.* 20:683–693.

Carlton, J.G., and P.J. Cullen. 2005. Sorting nexins. *Curr. Biol.* 15:R819–R820.

Carlton, J., M. Bujny, B.J. Peter, V.M. Oorschot, A. Rutherford, H. Mellor, J. Klumperman, H.T. McMahon, and P.J. Cullen. 2004. Sorting nexin-1 mediates tubular endosome-to-TGN transport through coincidence sensing of high-curvature membranes and 3-phosphoinositides. *Curr. Biol.* 14:1791–1800.

Carlton, J., M. Bujny, A. Rutherford, and P. Cullen. 2005a. Sorting nexins–unifying trends and new perspectives. *Traffic.* 6:75–82.

Carlton, J.G., M.V. Bujny, B.J. Peter, V.M. Oorschot, A. Rutherford, R.S. Arkell, J. Klumperman, H.T. McMahon, and P.J. Cullen. 2005b. Sorting nexin-2 is associated with tubular elements of the early endosome, but is not essential for retromer-mediated endosome-to-TGN transport. *J. Cell Sci.* 118:4527–4539.

Carroll, K.S., J. Hanna, I. Simon, J. Krise, P. Barbero, and S.R. Pfeffer. 2001. Role of Rab9 GTPase in facilitating receptor recruitment by TIP47. *Science.* 292:1373–1376.

Chavrier, P., R.G. Parton, H.P. Hauri, K. Simons, and M. Zerial. 1990. Localization of low molecular weight GTP binding proteins to exocytic and endocytic compartments. *Cell.* 62:317–329.

Christoforidis, S., and M. Zerial. 2000. Purification and identification of novel Rab effectors using affinity chromatography. *Methods.* 20:403–410.

Christoforidis, S., H.M. McBride, R.D. Burgoyne, and M. Zerial. 1999a. The Rab5 effector EEA1 is a core component of endosome docking. *Nature.* 397:621–625.

Christoforidis, S., M. Miaczynska, K. Ashman, M. Wilm, L. Zhao, S.C. Yip, M.D. Waterfield, J.M. Backer, and M. Zerial. 1999b. Phosphatidylinositol-3-OH kinases are Rab5 effectors. *Nat. Cell Biol.* 1:249–252.

Collins, B.M., C.F. Skinner, P.J. Watson, M.N. Seaman, and D.J. Owen. 2005. Vps29 has a phosphoesterase fold that acts as a protein interaction scaffold for retromer assembly. *Nat. Struct. Mol. Biol.* 12:594–602.

Cozier, G.E., J. Carlton, A.H. McGregor, P.A. Gleeson, R.D. Teasdale, H. Mellor, and P.J. Cullen. 2002. The phox homology (PX) domain-dependent, 3-phosphoinositide-mediated association of sorting nexin-1 with an early sorting endosomal compartment is required for its ability to regulate epidermal growth factor receptor degradation. *J. Biol. Chem.* 277:48730–48736.

Cullen, P.J. 2008. Endosomal sorting and signalling: an emerging role for sorting nexins. *Nat. Rev. Mol. Cell Biol.* 9:574–582.

Damen, E., E. Nielsen, J.E. Eygensteyn, and J.E. van Leeuwen. 2006. The human Vps29 retromer component is a metallo-phosphoesterase for a cation-independent mannose 6-phosphate receptor substrate peptide. *Biochem. J.* 398:399–409.

Deinhardt, K., S. Salinas, C. Verastegui, R. Watson, D. Worth, S. Hanrahan, C. Bucci, and G. Schiavo. 2006. Rab5 and Rab7 control endocytic sorting along the axonal retrograde transport pathway. *Neuron.* 52:293–305.

Futter, C.E., A. Gibson, E.H. Allchin, S. Maxwell, L.J. Ruddock, G. Odorizzi, D. Domingo, I.S. Trowbridge, and C.R. Hopkins. 1998. In polarized MDCK cells basolateral vesicles arise from clathrin-γ-adaptin-coated domains on endosomal tubules. *J. Cell Biol.* 141:611–623.

Gillooly, D.J., I.C. Morrow, M. Lindsay, R. Gould, N.J. Bryant, J.M. Gaullier, R.G. Parton, and H. Stenmark. 2000. Localization of phosphatidylinositol 3-phosphate in yeast and mammalian cells. *EMBO J.* 19:4577–4588.

Gokool, S., D. Tattersall, J.V. Reddy, and M.N. Seaman. 2007. Identification of a conserved motif required for Vps35p/Vps26p interaction and assembly of the retromer complex. *Biochem. J.* 408:287–295.

Gullapalli, A., T.A. Garrett, M.M. Paing, C.T. Griffin, Y. Yang, and J. Trejo. 2004. A role for sorting nexin 2 in epidermal growth factor receptor down-regulation: evidence for distinct functions of sorting nexin 1 and 2 in protein trafficking. *Mol. Biol. Cell.* 15:2143–2155.

Haft, C.R., M. de la Luz Sierra, R. Bafford, M.A. Lesniak, V.A. Barr, and S.I. Taylor. 2000. Human orthologs of yeast vacuolar protein sorting proteins Vps26, 29, and 35: assembly into multimeric complexes. *Mol. Biol. Cell.* 11:4105–4116.

Hierro, A., A.L. Rojas, R. Rojas, N. Murthy, G. Effantin, A.V. Kajava, A.C. Steven, J.S. Bonifacino, and J.H. Hurley. 2007. Functional architecture of the retromer cargo-recognition complex. *Nature.* 449:1063–1067.

Hirst, J., M.N. Seaman, S.I. Buschow, and M.S. Robinson. 2007. The role of cargo proteins in GGA recruitment. *Traffic.* 8:594–604.

Huang, F., A. Khvorova, W. Marshall, and A. Sorkin. 2004. Analysis of clathrin-mediated endocytosis of epidermal growth factor receptor by RNA interference. *J. Biol. Chem.* 279:16657–16661.

Johansson, M., M. Lehto, K. Tanhuanpaa, T.L. Cover, and V.M. Olkkonen. 2005. The oxysterol-binding protein homologue ORP1L interacts with Rab7 and alters functional properties of late endocytic compartments. *Mol. Biol. Cell.* 16:5480–5492.

Johansson, M., N. Rocha, W. Zwart, I. Jordens, L. Janssen, C. Kuijl, V.M. Olkkonen, and J. Neefjes. 2007. Activation of endosomal dynein motors by stepwise assembly of Rab7–RILP–p150[Glued], ORP1L, and the receptor βIll spectrin. *J. Cell Biol.* 176:459–471.

Kametaka, S., R. Mattera, and J.S. Bonifacino. 2005. Epidermal growth factor-dependent phosphorylation of the GGA3 adaptor protein regulates its recruitment to membranes. *Mol. Cell. Biol.* 25:7988–8000.

Kornfeld, S. 1992. Structure and function of the mannose 6-phosphate/insulin-like growth factor II receptors. *Annu. Rev. Biochem.* 61:307–330.

Mardones, G.A., P.V. Burgos, D.A. Brooks, E. Parkinson-Lawrence, R. Mattera, and J.S. Bonifacino. 2007. The trans-Golgi network accessory protein p56 promotes long-range movement of GGA/clathrin-containing transport carriers and lysosomal enzyme sorting. *Mol. Biol. Cell.* 18:3486–3501.

Mari, M., M.V. Bujny, D. Zeuschner, W.J. Geerts, J. Griffith, C.M. Petersen, P.J. Cullen, J. Klumperman, and H.J. Geuze. 2008. SNX1 defines an early endosomal recycling exit for sortilin and mannose 6-phosphate receptors. *Traffic.* 9:380–393.

Nakada-Tsukui, K., Y. Saito-Nakano, V. Ali, and T. Nozaki. 2005. A retromer-like complex is a novel Rab7 effector that is involved in the transport of the virulence factor cysteine protease in the enteric protozoan parasite *Entamoeba histolytica. Mol. Biol. Cell.* 16:5294–5303.

Neeft, M., M. Wieffer, A.S. de Jong, G. Negroiu, C.H. Metz, A. van Loon, J. Griffith, J. Krijgsveld, N. Wulffraat, H. Koch, et al. 2005. Munc13-4 is an effector of rab27a and controls secretion of lysosomes in hematopoietic cells. *Mol. Biol. Cell.* 16:731–741.

Nothwehr, S.F., P. Bruinsma, and L.A. Strawn. 1999. Distinct domains within Vps35p mediate the retrieval of two different cargo proteins from the yeast prevacuolar/endosomal compartment. *Mol. Biol. Cell.* 10:875–890.

Nothwehr, S.F., S.A. Ha, and P. Bruinsma. 2000. Sorting of yeast membrane proteins into an endosome-to-Golgi pathway involves direct interaction of their cytosolic domains with Vps35p. *J. Cell Biol.* 151:297–310.

Panaretou, C., J. Domin, S. Cockcroft, and M.D. Waterfield. 1997. Characterization of p150, an adaptor protein for the human phosphatidylinositol (PtdIns) 3-kinase. Substrate presentation by phosphatidylinositol transfer protein to the p150.Ptdins 3-kinase complex. *J. Biol. Chem.* 272:2477–2485.

Peden, A.A., V. Oorschot, B.A. Hesser, C.D. Austin, R.H. Scheller, and J. Klumperman. 2004. Localization of the AP-3 adaptor complex defines a novel endosomal exit site for lysosomal membrane proteins. *J. Cell Biol.* 164:1065–1076.

Popoff, V., G.A. Mardones, D. Tenza, R. Rojas, C. Lamaze, J.S. Bonifacino, G. Raposo, and L. Johannes. 2007. The retromer complex and clathrin define an early endosomal retrograde exit site. *J. Cell Sci.* 120:2022–2031.

Press, B., Y. Feng, B. Hoflack, and A. Wandinger-Ness. 1998. Mutant Rab7 causes the accumulation of cathepsin D and cation-independent mannose 6-phosphate receptor in an early endocytic compartment. *J. Cell Biol.* 140:1075–1089.

Raposo, G., M.J. Kleijmeer, G. Posthuma, J.W. Slot, and H.J. Geuze. 1997. Immunogold labeling of ultrathin cryosections: application in immunology. *In* Weir's Handbook of Experimental Immunology. Fifth edition. Vol. 4. D. Weir, L.A. Herzenberg, and C. Blackwell, editors. Blackwell Science, Cambridge, MA. 1–11.

Reinacher-Schick, A., and B.M. Gumbiner. 2001. Apical membrane localization of the adenomatous polyposis coli tumor suppressor protein and subcellular distribution of the β-catenin destruction complex in polarized epithelial cells. *J. Cell Biol.* 152:491–502.

Rink, J., E. Ghigo, Y. Kalaidzidis, and M. Zerial. 2005. Rab conversion as a mechanism of progression from early to late endosomes. *Cell.* 122:735–749.

Rojas, R., S. Kametaka, C.R. Haft, and J.S. Bonifacino. 2007. Interchangeable but essential functions of SNX1 and SNX2 in the association of retromer with endosomes and the trafficking of mannose 6-phosphate receptors. *Mol. Cell. Biol.* 27:1112–1124.

Sakane, A., S. Hatakeyama, and T. Sasaki. 2007. Involvement of Rabring7 in EGF receptor degradation as an E3 ligase. *Biochem. Biophys. Res. Commun.* 357:1058–1064.

Sato, M., K. Sato, P. Fonarev, C.J. Huang, W. Liou, and B.D. Grant. 2005. *Caenorhabditis elegans* RME-6 is a novel regulator of RAB-5 at the clathrin-coated pit. *Nat. Cell Biol.* 7:559–569.

Seaman, M.N. 2004. Cargo-selective endosomal sorting for retrieval to the Golgi requires retromer. *J. Cell Biol.* 165:111–122.

Seaman, M.N. 2005. Recycle your receptors with retromer. *Trends Cell Biol.* 15:68–75.

Seaman, M.N. 2007. Identification of a novel conserved sorting motif required for retromer-mediated endosome-to-TGN retrieval. *J. Cell Sci.* 120:2378–2389.

Seaman, M.N., J.M. McCaffery, and S.D. Emr. 1998. A membrane coat complex essential for endosome-to-Golgi retrograde transport in yeast. *J. Cell Biol.* 142:665–681.

Shi, H., R. Rojas, J.S. Bonifacino, and J.H. Hurley. 2006. The retromer subunit Vps26 has an arrestin fold and binds Vps35 through its C-terminal domain. *Nat. Struct. Mol. Biol.* 13:540–548.

Sonnichsen, B., S. De Renzis, E. Nielsen, J. Rietdorf, and M. Zerial. 2000. Distinct membrane domains on endosomes in the recycling pathway visualized by multicolor imaging of Rab4, Rab5, and Rab11. *J. Cell Biol.* 149:901–914.

Stein, M.P., Y. Feng, K.L. Cooper, A.M. Welford, and A. Wandinger-Ness. 2003. Human VPS34 and p150 are Rab7 interacting partners. *Traffic.* 4:754–771.

Strochlic, T.I., T.G. Setty, A. Sitaram, and C.G. Burd. 2007. Grd19/Snx3p functions as a cargo-specific adapter for retromer-dependent endocytic recycling. *J. Cell Biol.* 177:115–125.

Theos, A.C., D. Tenza, J.A. Martina, I. Hurbain, A.A. Peden, E.V. Sviderskaya, A. Stewart, M.S. Robinson, D.C. Bennett, D.F. Cutler, et al. 2005. Functions of adaptor protein (AP)-3 and AP-1 in tyrosinase sorting from endosomes to melanosomes. *Mol. Biol. Cell.* 16:5356–5372.

Ullrich, O., H. Horiuchi, C. Bucci, and M. Zerial. 1994. Membrane association of Rab5 mediated by GDP-dissociation inhibitor and accompanied by GDP/GTP exchange. *Nature.* 368:157–160.

Vonderheit, A., and A. Helenius. 2005. Rab7 associates with early endosomes to mediate sorting and transport of Semliki forest virus to late endosomes. *PLoS Biol.* 3:e233.

Wang, D., M. Guo, Z. Liang, J. Fan, Z. Zhu, J. Zang, Z. Zhu, X. Li, M. Teng, L. Niu, et al. 2005. Crystal structure of human vacuolar protein sorting protein 29 reveals a phosphodiesterase/nuclease-like fold and two protein-protein interaction sites. *J. Biol. Chem.* 280:22962–22967.

Zhong, Q., C.S. Lazar, H. Tronchere, T. Sato, T. Meerloo, M. Yeo, Z. Songyang, S.D. Emr, and G.N. Gill. 2002. Endosomal localization and function of sorting nexin 1. *Proc. Natl. Acad. Sci. USA.* 99:6767–6772.

Zhong, Q., M.J. Watson, C.S. Lazar, A.M. Hounslow, J.P. Waltho, and G.N. Gill. 2005. Determinants of the endosomal localization of sorting nexin 1. *Mol. Biol. Cell.* 16:2049–2057.